optica

Room-temperature fiber laser at 3.92 μm

Frédéric Maes,[1,*] Vincent Fortin,[1] Samuel Poulain,[2] Marcel Poulain,[2] Jean-Yves Carrée,[2] Martin Bernier,[1] and Réal Vallée[1]

[1]Center for Optics, Photonics and Lasers (COPL), Université Laval, Québec, Québec G1V 0A6, Canada
[2]Le Verre Fluoré, Campus KerLann, F-35170 Bruz, Brittany, France
*Corresponding author: frederic.maes.1@ulaval.ca

Received 13 March 2018; revised 1 June 2018; accepted 4 June 2018 (Doc. ID 325994); published 22 June 2018

Rare-earth-doped fiber lasers are promising contenders in the development of spectroscopy, free-space communications, and countermeasure applications in the 3–5 μm spectral region. However, given the limited transparency of the commonly used fluorozirconate glass fiber, these systems have only achieved wavelength coverage up to 3.8 μm, hence fueling the development of more suitable fiber glass compositions. To this extent, we propose in this Letter a novel heavily holmium-doped fluoroindate fiber, providing extended transparency up to 5 μm, to demonstrate the longest wavelength room-temperature fiber laser at 3.92 μm. Achieving ∼200 mW of output power when cladding pumped by a commercial 888 nm laser diode, this demonstration paves the way for powerful mid-infrared fiber lasers emitting at and beyond 4 μm.

OCIS codes: (060.2320) Fiber optics amplifiers and oscillators; (060.3510) Lasers, fiber; (140.3070) Infrared and far-infrared lasers; (060.2290) Fiber materials.

https://doi.org/10.1364/OPTICA.5.000761

Fiber lasers (FLs) find many applications in the medical, spectroscopy, and manufacturing fields owing to their diffraction-limited beam quality as well as their rugged, maintenance-free, and small-footprint design [1]. However, extending the wavelength coverage of FLs in the mid-infrared (MIR) region, especially above 3 μm, while maintaining significant output power is an ongoing challenge. This spectral region has gathered much attention owing to the presence of fundamental molecular absorption bands enabling spectroscopy and remote sensing applications [2]. In addition, its overlap with the atmospheric transmission window at 3.9 μm is of particular interest for countermeasure and free-space communication applications [3,4].

Given the large number of optical transitions offered by rare-earth (RE)-doped glasses, RE-doped fibers have demonstrated significant wavelength coverage in the MIR, as shown in Fig. 1. At wavelengths around 2 μm, near-infrared diode-pumped thulium (Tm^{3+})-doped silica FLs have reached the kilowatt output power level, an achievement made possible by the availability of high-power fiber-based components as well as the high mechanical and thermal strength of silica fibers [5]. However, the limited transmission and high phonon energy (1100 cm^{-1}) of silica-based fibers render laser emission above 2.2 μm very unlikely [4]. Fluorozirconate (ZrF_4)-based fibers, on the other hand, possess a relatively low phonon energy of 574 cm^{-1} that sets their infrared transmission edge around 4 μm [4]. They have been the most successful in the demonstration of MIR laser emission above 2.4 μm, as seen in Fig. 1. Indeed, using core written fiber Bragg gratings (FBGs) [6] as well as single-mode splices, near-infrared-pumped erbium (Er^{3+})-doped monolithic all-fiber lasers have been demonstrated at both 2.94 μm and 3.55 μm, with output powers of 30 and 5.6 W, respectively [7,8]. Additionally, 1.06 W at 3.15 μm has been demonstrated in a free-space in-band core-pumped dysprosium (Dy^{3+})-doped ZrF_4 fiber laser [9] and 4 mW were achieved at 3.78 μm by stretching to its limit the 3.5 μm transition in Er^{3+}:ZrF_4 fibers [10]. Finally, the longest wavelength achieved from a fiber laser, to date, was reported two decades ago by Schneider *et al.*, who demonstrated 11 mW of output power at 3.9 μm on the $^5I_5 \rightarrow {}^5I_6$ transition of a holmium (Ho^{3+})-doped ZrF_4 fiber [11]. However, this demonstration had the major drawback of requiring both liquid nitrogen cooling as well as core pumping by a Ti:Sapphire laser to achieve threshold, hence revealing the shortcoming of RE-doped ZrF_4 fiber lasers in terms of MIR wavelength coverage. This shortcoming stems from the phonon-related properties of ZrF_4-based glasses that prevent laser emission to longer wavelengths for two main reasons: first, because the emission of RE ions is quenched by multi-phonon (MP) decay, which increases exponentially with both temperature and emission wavelength [12]; second, laser emission at longer wavelengths is also hampered by the transparency of the ZrF_4 glass, which rapidly falls off around 4 μm. Therefore, different RE-doped glass matrices have been sought in order to provide suitable optical properties for laser emission around and beyond 4 μm. Now, the recent availability of a new generation of low-loss and heavily RE-doped InF_3 glass fibers with a transmission window extending up to 5 μm represents a crucial step towards a new generation of MIR fiber lasers.

Accordingly, we report here the longest-wavelength room-temperature diode-pumped fiber laser operating at 3.92 μm based on a novel holmium-doped fluoroindate glass fiber (Ho^{3+}:InF_3).

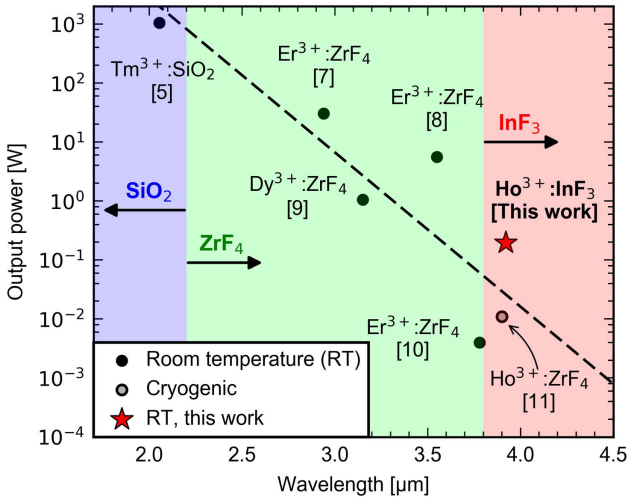

Fig. 1. Record continuous-wave output powers from room-temperature RE-doped MIR FLs with respect to emitted wavelength.

Relying on a high Ho^{3+} concentration to enhance ion-pair energy transfer upconversion (ETU) processes and on excited state absorption (ESA) at the pump wavelength, the free-running cavity produces nearly 200 mW of output power with a slope efficiency of around 10% with respect to the launched 888 nm cladding pump power. This demonstration shows the benefits of using InF_3 fibers to unlock room-temperature emission of long-wavelength transitions in RE ions and heralds a new generation of MIR FLs emitting near 3.9 μm and above.

The partial energy level diagram of the Ho^{3+}:InF_3 system, along with relevant physical processes, is presented in Fig. 2(a), where on the right-hand side, the lifetimes of the different energy levels are given. Ground state absorption (GSA) at 888 nm on the $^5I_8 \rightarrow {}^5I_5$ transition provides direct pumping of the upper laser level of the 3.9 μm transition [13]. Figure 2(c) presents the cross section of this transition, which peaks around 888 nm at a value of 4.3×10^{-26} m^{-2}. Such pumping wavelength is readily available through high-power commercial multimode laser diodes and offers a simple and convenient approach to generate 3.9 μm emission in Ho^{3+}:InF_3 fibers. Laser emission around 3.9 μm occurs between two excited levels of the Ho^{3+}:InF_3 system on the $^5I_5 \rightarrow {}^5I_6$ transition. The cross section of this transition has been measured in bulk Ho^{3+}:InF_3 as previously reported in [13] and is presented in Fig. 2(b). One can see that it spans from 3840 to 4020 nm, overlapping the atmosphere's transmission window at 3.9 μm [3], and possesses a peak cross section of 3.4×10^{-25} m^{-2} around 3.92 μm. The lifetime, including radiative and non-radiative decay, of the upper laser level $^5I_5$ in Ho^{3+}:InF_3 bulks has been measured to be 135 μs. For comparison, the measured lifetime of the same level in Ho^{3+}:ZrF_4 bulks is 43 μs, a decrease mostly attributed to the higher phonon energy of ZrF_4 (574 cm^{-1}) compared to that of InF_3 (509 cm^{-1}) [16]. Nonetheless, the 3.9 μm transition in Ho^{3+}:InF_3 glasses remains self-terminated, since the lifetime of the lower level ($^5I_6$) is 46 times longer than that of the upper level. However, recent spectroscopic studies have suggested that this limitation could be alleviated by using high Ho^{3+} concentrations to enhance ETU processes [14]. Moreover, excited state absorption (ESA) at 888 nm can also occur on the $^5I_7 \rightarrow {}^5F_5$ transition [15], a process that has a two-fold effect on the 3.9 μm laser efficiency. Not only does it counteract ion bottlenecking in the long-lived $^5I_7$ level, it actually upconverts ions from the latter level to the $^5F_5$ level, which then undergo MP decay to level $^5I_5$. Among the different energy transfers that have been reported in Ho^{3+}:InF_3 [14], the one illustrated in Fig. 2(a) (i.e., $^5I_6$, $^5I_6 \rightarrow {}^5I_8$, $^5F_5$) appears to be the most beneficial for laser emission at 3.9 μm. This ETU contributes to the population inversion of the 3.9 μm transition, since it removes two ions from the lower energy level $^5I_6$ and recycles one of those ions back to the upper laser level $^5I_5$. A similar recycling mechanism is already exploited to increase the efficiency of the self-terminated $^4I_{11/2} \rightarrow {}^4I_{13/2}$ transition in highly doped Er^{3+}:ZrF_4 fiber lasers at 2.8 μm [17].

The schematic of the 3.92 μm room-temperature fiber laser reported here is depicted in Fig. 3. The fiber cavity is made of a 23 cm long 10 mol. % Ho^{3+}:InF_3 double-clad fiber developed by *Le Verre Fluoré*. A short length of fiber was selected to limit potential signal reabsorption from the lower level of the transition, which can occur for insufficient pumping [13]. The measured fiber core's molar composition is

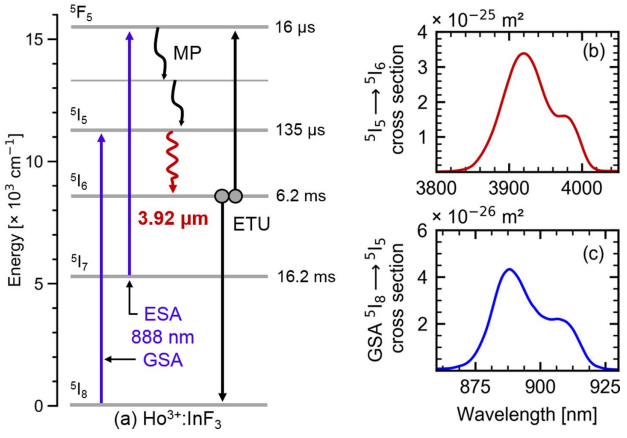

Fig. 2. (a) Energy level diagram of the Ho^{3+}:InF_3 system with relevant physical processes; (b) cross section of the $^5I_5 \rightarrow {}^5I_6$ emission; and (c) cross section of the $^5I_8 \rightarrow {}^5I_5$ absorption reported in [13–15]. GSA, ground state absorption; ESA, excited state absorption; ETU, energy transfer upconversion.

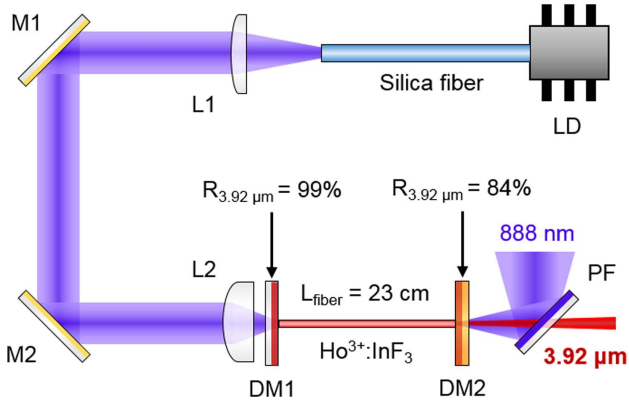

Fig. 3. Experimental setup of the room-temperature fiber laser at 3.92 μm. LD, 888 nm multimode laser diode; L1–L2, lenses in 1:2 de-magnification configuration; M1–M2, gold-sputtered mirrors; DM1, home-sputtered quartz dichroic mirror; DM2, home-sputtered ZnSe dichroic mirror; PF, pump filter.

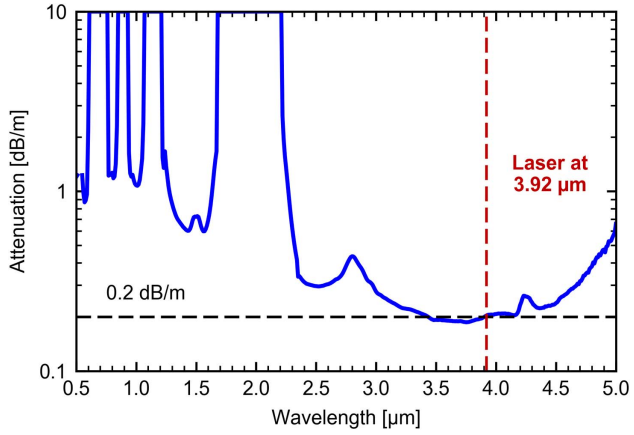

Fig. 4. Core attenuation of the Ho^{3+}:InF_3 fiber from 0.5 to 5.0 μm measured by cutback.

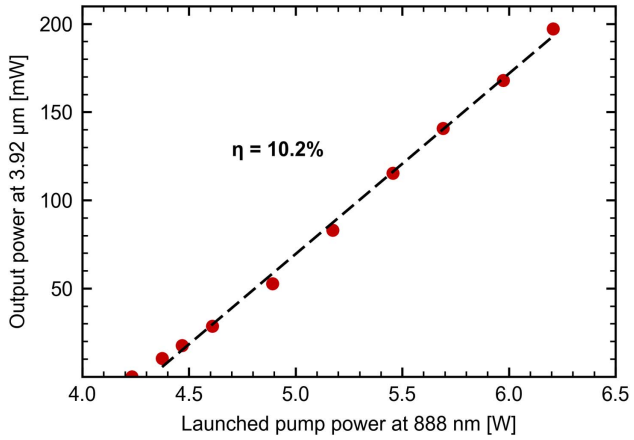

Fig. 5. Output power at 3.92 μm with respect to the launched pump power.

$31InF_3$-$30.5BaF_2$-$19ZnF_2$-$9.5SrF_2$-$10HoF_3$, while the cladding's molar composition is $41InF_3$-$33BaF_2$-$18ZnF_2$-$8SrF_2$. The slightly multimode fiber core has a diameter of 16 μm and a numerical aperture (NA) of 0.2. The cladding has a circular diameter of 100 μm truncated by two parallel flats separated by 90 μm to enhance cladding pump absorption, and is coated with a low-index fluoroacrylate providing multimode guidance (NA > 0.4) at 890 nm. As seen in Fig. 4, the core attenuation of the drawn fiber is lying below 0.2 dB/m over the 3.4–4.0 μm spectral region, making the InF_3 fiber particularly suited for laser emission around 3.9 μm.

The Ho^{3+}:InF_3 fiber cavity was bounded by two dichroic mirrors (DMs). The entrance DM1, providing 87% transmission at 888 nm and a broadband 99% reflectivity around 3.9 μm, was deposited on a quartz substrate, while the output DM2 was fabricated on a ZnSe substrate with a reflectivity of 84% around 3.9 μm and 15% at 888 nm. The right-angled cleaved endfaces of the Ho^{3+}:InF_3 fiber were secured in copper v-grooves with ultraviolet (UV)-cured low-index polymer and were butted against the DMs using precision alignment stages. Optical pumping at 888 nm was provided by a multimode laser diode (LD, nLight element e03) pigtailed to a 200/220 0.22 NA silica fiber. A set of lenses (L1, L2) in a 1:2 de-magnification configuration and gold mirrors (M1, M2) enabled the injection of the pump through the entrance DM1 into the cladding of the Ho^{3+}:InF_3 fiber. Through a standard cutback measurement, the cladding absorption at 888 nm and the pump launch efficiency were measured to be 7.7 dB/m and 45%, respectively. An aluminum plate was used to passively cool the length of the fiber, while fans provided forced convection to cool down the fiber tips protruding from the copper v-grooves.

The output power at 3.9 μm was measured with a low-power thermopile detector (Gentec EO, model XLP12-3S-H2) along with a pump filter (PF) to reject the residual pump power. The spectrum was analyzed by a mid-infrared optical spectrum analyzer (Yokogawa, model AQ6376, with extended wavelength coverage up to 5000 nm) at a spectral resolution of 0.2 nm.

The 3.92 μm output power as a function of the launched pump power at 888 nm is presented in Fig. 5. The laser threshold is located at 4.3 W, while the slope efficiency is 10.2%. Based on the single-pass pump absorption measured through cutback, the efficiency with respect to the absorbed pump power was estimated to be around 24%, i.e., close to the system's Stokes efficiency of 23%. It should be noted that the Stokes efficiency does not take into account excitation recycling through ETU, a phenomenon that has been show numerically and experimentally to allow heavily doped fiber lasers to exceed the Stokes efficiency [17,18]. A record output power of 197 mW was achieved for a launched pump power of 6.2 W. Above this pump level, the cavity underwent failure at the butt-coupling between the fiber and the entrance DM1 due to an excess heat load. Figure 6 displays the laser output spectrum for various output powers. As can be seen, the free-running cavity emits on four different laser lines between 3917 and 3924 nm that are located near the peak of the emission cross section measured in Ho^{3+}:InF_3 bulks having an identical glass composition [13]. Broad wavelength scans did not reveal any spectral features near 2.1 and 2.9 μm, which could have been generated from transitions from lower-lying energy levels. These transitions were possibly hindered by ESA and ETU processes illustrated in Fig. 2, to the benefit of the 3.9 μm transition.

When the pump diode was operated at low powers, the fluorescence emitted by the Ho^{3+}:InF_3 fiber had a vivid red color. As the power of the pump was increased, the red fluorescence increased accordingly, while additional visible components were

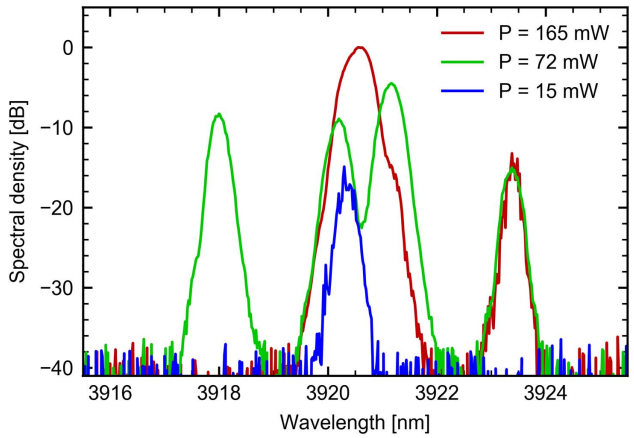

Fig. 6. Spectrum of the Ho^{3+}:InF_3 fiber laser for different output powers.

seen to give more of a pink glow to the fiber. At the maximum launched pump power of 6.2 W, green visible fluorescence was clearly observed at the input of the Ho^{3+}:InF_3 cavity. The evolution of the fiber color gives an insight into the kinetics of the local energy level populations. The constant red fluorescence emitted by the Ho^{3+} ions corresponds to spontaneous radiative decay to the ground state originating from the $^5F_5$ level, therefore indicating a population buildup in this level. This observation is in agreement with the energy level diagram depicted in Fig. 2, where ESA at 888 nm from the $^5I_7$ level and ETU from the $^5I_6$ level are seen to promote ions to the $^5F_5$ level. Moreover, the red fluorescence suggests that the contribution of ESA and ETU is increasing the efficiency of the 3.9 μm laser by enabling recycling of the pump excitation and limiting ion bottlenecking in lower-lying energy levels ($^5I_7$, $^5I_6$). As for the additional visible fluorescent components emitted by the fiber at higher pumping levels, spectroscopic investigations on Ho^{3+}:ZrF_4 bulks suggest that they are the result of a second ESA at 888 nm originating from level $^5I_5$ [15]. Furthermore, the benefit of ESA at 888 nm ($^4I_7 \rightarrow {}^4F_5$) and ETU on the 3.9 μm transition was investigated through preliminary numerical modeling. Although the accuracy of the model is seriously limited, given that crucial spectroscopic parameters are currently unknown, the model clearly shows that no gain can be achieved if ETU does not occur. Moreover, while ESA alone is not sufficient to produce gain at 3.9 μm, modeling also confirms the benefit of ESA on the gain when ETU occurs.

Nonetheless, in order to clearly assess the contribution of the different ESAs and ETUs on the 3.9 μm transition, additional spectroscopic investigations, supported by numerical modeling, need to be conducted. Simultaneously, laser experiments with low Ho^{3+}-doping concentration InF_3 fibers will be carried out to further clarify the impact of ETUs on 3.9 μm laser emission. Such low-doping-concentration fibers may also provide a simple pathway to mitigate heat-load-related failure of the cavity. Furthermore, laser emission at 3.9 μm with currently available Ho^{3+}:ZrF_4 fibers may be attempted to evaluate the direct benefit of InF_3 fibers on long-wavelength MIR transitions. Given the significant progress of ZrF_4 fiber lasers at 2.8 μm in the last decade stemming from improvement in the fiber composition and manufacturing, state-of-the-art Ho^{3+}:ZrF_4 fibers may allow more efficient performances at 3.9 μm than those reported two decades ago [11].

Future research will also be devoted to the power-scaling of the laser system. To this extent, the cladding of the Ho^{3+}:InF_3 fiber will be increased in order to increase the pump launch efficiency and reduce the heat load at the launch site. Meanwhile, the core's diameter and NA will be optimized in order to maintain a high pump excitation density to activate energy recycling processes, while ensuring single-mode operation at 3.9 μm. The inscription of FBGs in the core of the InF_3 fiber by a femtosecond laser will also be developed to eliminate the need for bulk reflectors at 3.9 μm and enable the use of more efficient passive cooling methods. Simultaneously, low-loss splice processes will allow all-fiber pump delivery and will further mitigate the heat load at the pump launch site. We believe such implementations will lead to watt-level monolithic all-fiber cavities at 3.9 μm, a design that has shown unparalleled output power, efficiency, and stability at 2.9 and 3.5 μm [7,8].

In summary, we have reported in this Letter the longest-wavelength room-temperature fiber laser. Based on a novel 10 mol. % Ho^{3+}:InF_3 fiber, cladding pumped by an 888 nm commercial laser diode, the free-running cavity provides 197 mW of output power at 3.92 μm with a slope efficiency of 10.2% with respect to the launched pump power. This feat is likely enabled by excitation recycling processes enhanced by the high Ho^{3+}-doping concentration as well as by the extended transparency (>5 μm) and the lower phonon energy of the InF_3 fiber. We believe that this demonstration will spark the development of a new generation of RE-doped InF_3 fiber laser systems operating at 3.9 μm and beyond, which will address the unfulfilled needs of MIR applications in the 3–5 μm spectral region.

Funding. Natural Sciences and Engineering Research Council of Canada (NSERC) (IRCPJ469414-13); Canada Foundation for Innovation (CFI) (5180); Fonds de Recherche du Québec—Nature et Technologies (FRQNT) (144616).

Acknowledgment. We thank the Yokogawa Test & Measurement Corporation, for providing the OSA used for the spectral measurements, as well as Souleymane T. Bah and Marc D'Auteuil for their contributions in fabricating the dichroic mirrors.

REFERENCES

1. D. J. Richardson, J. Nilsson, and W. A. Clarkson, J. Opt. Soc. Am. B **27**, B63 (2010).
2. A. Schliesser, N. Picqué, and T. W. Hänsch, Nat. Photonics **6**, 440 (2012).
3. H. H. P. T. Bekman, J. C. van den Heuvel, F. J. M. van Putten, and R. Schleijpen, Proc. SPIE **5615**, 27 (2004).
4. S. D. Jackson, Nat. Photonics **6**, 423 (2012).
5. T. Ehrenreich, R. Leveille, I. Majid, K. Tankala, G. Rines, and P. Moulton, Proc. SPIE **7580**, 758016 (2010).
6. M. Bernier, D. Faucher, R. Vallée, A. Saliminia, G. Androz, Y. Sheng, and S. L. Chin, Opt. Lett. **32**, 454 (2007).
7. V. Fortin, M. Bernier, S. T. Bah, and R. Vallée, Opt. Lett. **40**, 2882 (2015).
8. F. Maes, V. Fortin, M. Bernier, and R. Vallée, Opt. Lett. **42**, 2054 (2017).
9. R. I. Woodward, M. R. Majewski, G. Bharathan, D. D. Hudson, A. Fuerbach, and S. D. Jackson, Opt. Lett. **43**, 1471 (2018).
10. O. H. Sapir, S. D. Jackson, and D. Ottaway, Opt. Lett. **41**, 1676 (2016).
11. J. Schneider, C. Carbonnier, and U. B. Unrau, Appl. Opt. **36**, 8595 (1997).
12. L. A. Riseberg and H. W. Moos, Phys. Rev. **174**, 429 (1968).
13. L. Gomes, V. Fortin, M. Bernier, R. Vallée, S. Poulain, M. Poulain, and S. D. Jackson, Opt. Mater. **60**, 618 (2016).
14. L. Gomes, V. Fortin, M. Bernier, F. Maes, R. Vallée, S. Poulain, M. Poulain, and S. D. Jackson, Opt. Mater. **66**, 519 (2017).
15. D. Piatkowski, K. Wisniewski, M. Rozanski, C. Koepke, M. Kaczkan, M. Klimczak, R. Piramidowicz, and M. Malinowski, J. Phys. **20**, 155201 (2008).
16. A. Akella, E. A. Downing, and L. Hesselink, J. Non-Cryst. Solids **213–214**, 1 (1997).
17. M. Pollnau and S. D. Jackson, IEEE J. Quantum Electron. **38**, 162 (2002).
18. D. Faucher, M. Bernier, G. Androz, N. Caron, and R. Vallée, Opt. Lett. **36**, 1104 (2011).